Submitted, accepted and published by
Fuel Processing Technology 171 (2018) 78–88

RELEVANCE OF PLANT DESING ON CLC PROCESS PERFORMANCE USING A Cu-BASED OXYGEN CARRIER

Alberto Abad*, Pilar Gayán, Francisco García-Labiano, Luis F. de Diego, Juan Adánez

Dept. of Energy and Environment, Instituto de Carboquímica (ICB-CSIC), Miguel Luesma Castán 4, Zaragoza 50018, Spain

*Email: *abad@icb.csic.es*

Abstract

Previously validated mathematical CLC models were used to simulate the process performance of CLC methane combustion using an impregnated Cu-based material and to analyse the effect of the fuel reactor design; being either a bubbling fluidized bed or a circulating fluidized bed. The CLC models considered both the fluid dynamic of the fluidized beds at the specific regime and the corresponding kinetics of oxygen carrier reduction. From the model outputs, the performance of the different systems was assessed by calculating the methane conversion in the fuel reactor. Main results highlights that the selection of a suitable particle size of the oxygen carrier and cross section area are key factors to achieve complete combustion with low solids inventory in the fuel reactor. In addition, the growing of bubbles should be limited in order to achieve high CH_4 conversion with low solids inventory values, mainly in the bubbling regime with low cross section areas. Complete combustion was predicted with solids inventory in the fuel reactor of 250 kg/MW_{th} (1 m^2/MW and particle size of 0.25 mm) or 125 kg/MW_{th} (0.2 m^2/MW and a particle size of 0.15 mm) in the bubbling and turbulent regime, respectively. Considering the pressure drop related to these conditions, conclusions for the optimization design of a CLC unit using the impregnated material are drawn based on the results of the modelling and simulation.

Keywords: CO_2 capture; Chemical Looping Combustion; Copper; Methane; Modelling; Fluidized Bed.

1. Introduction

Chemical Looping Combustion, CLC, is one of the most promising processes to capture CO_2 with low economic, energetic and environmental costs [1]. CLC is based on the transfer of the oxygen from air to the fuel by using a solid oxygen carrier. One of the most used configurations for CLC units is the use of two interconnected fluidized bed reactors, with the oxygen carrier material circulating between them; see Fig. 1. In the fuel reactor, the oxygen carrier is reduced while the fuel is oxidized. In the air reactor, the oxygen carrier is oxidized again with air to its original state. The net chemical reaction and combustion enthalpy is the same as in a conventional combustion, where the fuel is burned in direct contact with oxygen from air. It is highlighted that the CO_2 capture is inherent to the CLC process, as the air is not mixed with the fuel.

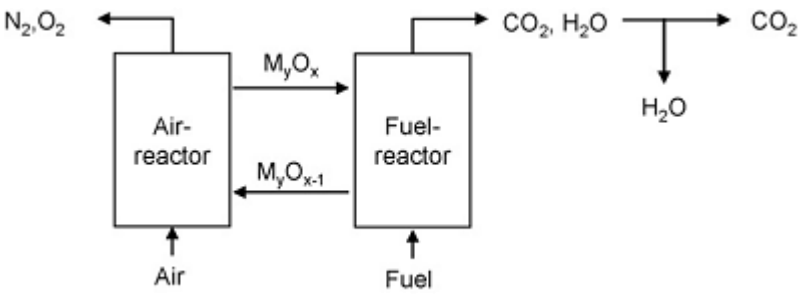

Fig. 1. Reactor scheme of the CLC process.

CLC technology for gaseous fuels has been successfully demonstrated with more than 4000 hours of operational experience in continuous CLC plants up to 150 kW_{th} using more than 40 different oxygen carriers [2]. Among them, a Cu-based material has been developed and selected as a promising material for the scale-up of the process [3]. This material was prepared by the impregnation method, which is adequate for production of large amounts of particles at low cost. Our research group at Instituto de Carboquímica (ICB-CSIC) has optimized the impregnation method to develop highly reactive Cu-based materials without

tendency towards agglomeration of particles during the operation in a fluidized bed [4]. This material is able to properly burn gaseous fuels such as syngas and CH_4, even with some fractions of impurities such as light hydrocarbon or H_2S [5-7]. In addition, evaluation of the operating conditions and selection of the alumina support has been performed with the target of improve the life-time of particles [8,9], which eventually has been estimated to be up to 5000 h for an optimized material [3]. A maximum temperature in the fuel reactor about 800-850 ºC is highly recommended, while the avoidance of $CuAl_2O_4$ formation can improve the durability of the particles.

Impregnated Cu-based oxygen carriers have been tested in several CLC facilities with promising results. These units can be classified depending on the fluid dynamic characteristics of the fuel reactor. Thus, 10 kW_{th} CLC units located at ICB-CSIC [10,11] and IFP [12] were designed for bubbling fluidized bed conditions in the fuel reactor, while the fuel reactor in the 120 kW_{th} unit and TUV [13-15] and 150 kW_{th} unit at SINTEF [16] were circulating fluidized beds. Recently, the 120 kW_{th} CLC unit at TUV has been modified to include a wider section in the bottom part of the reactor, but maintaining the circulation of solids in a narrow riser above the bottom bed [17]. Fig. 2 shows schemes of all these units where impregnated Cu-based oxygen carriers developed by ICB-CSIC have been tested.

When the fuel reactor was a bubbling fluidized bed reactor mode, complete combustion was achieved during operation in CLC units when the oxygen carrier to fuel ratio value was above $\phi = 1.5$ [6-11] whatever the particle size used in the 100-500 μm interval, and even with solids inventory values in the fuel reactor as low as 350 kg/MW_{th}. However, complete combustion was not achieved with these particles in circulating fluidized bed conditions, when maximum CH_4 conversion values of 70-80 % with solids inventory values in the 200-400 kg/MW_{th} interval [14]. But near complete CH_4 conversion has been achieved with 120 kg/MW_{th} in the fuel reactor when the particle size of impregnated materials was limited below 200 μm [16].

These results suggest that factors affecting to the fluid dynamic of the fuel reactor, such as gas velocity and particle size can affect to the performance of the oxygen carrier in a CLC unit.

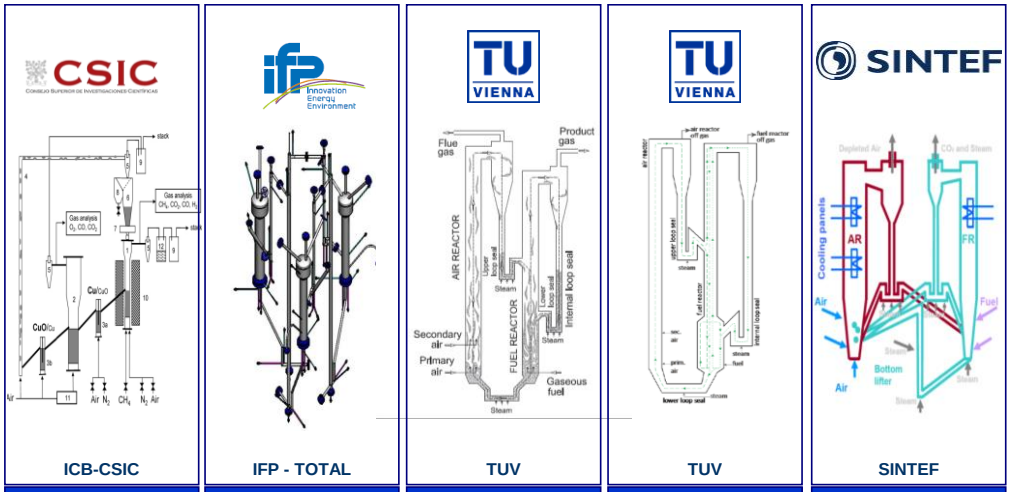

	ICB-CSIC	IFP - TOTAL	TUV	TUV	SINTEF
COUNTRY	SPAIN	FRANCE	AUSTRIA	AUSTRIA	NORWAY
Power (kW_{th})	10	10	120	120	150
Configuration	BFB-BFB	BFB-BFB-BFB	CFB-CFB	CFB-CFB	CFB-CFB
Operat. time (h)	200	160	100	25	n.a.

Fig. 2. Schemes of the CLC units where impregnated Cu-based oxygen carrier materials developed by ICB-CSIC have been tested [10-17]. BFB: bubbling fluidized bed; CFB: circulating fluidized bed.

The next challenge is to upscale the CLC technology from 150 kW_{th} to 10 MW_{th} since there is a promising niche application in on-field steam generation with carbon dioxide capture and storage (CCS). Successful upscaling of this technology is highly dependent on two key aspects, namely 1) upscaling of reactor system and 2) upscaling of oxygen carrier manufacture. Most efforts are being allocated to upscale the CLC system designs to the desired power of 10 MW_{th} [18]. Considering the results obtained in CLC plants above described, careful design of the fuel reactor must be considered to achieve the desired complete combustion of natural gas. In this sense, modelling is a relevant tool before the design, optimization and scale-up of the CLC process.

In this work, two theoretical models are used to analyse the relevance of the fuel reactor design on the performance of an impregnated Cu-based oxygen carrier burning methane in CLC. In this way, a CLC model for the fuel reactor in the 10 kW_{th} CLC unit at ICB-CSIC was developed for a bubbling fluidized bed. The second fuel reactor model was developed to simulate the 120 kW_{th} unit at TUV, where the fuel reactor was a circulating fluidized bed. Simulations of these CLC units allowed obtaining optimized conditions depending on the regime flow. From the results obtained, a brief discussion is included where relevant suggestions are drawn for a safe scale-up of the CLC process.

2. Mathematical models

Dedicated theoretical models for the fuel reactor were developed in Fortran Code® considering the geometry and operating conditions existing in both the 10 kW_{th} CLC unit at ICB-CSIC [10] and 120 kW_{th} CLC unit at TUV [14]. The bubbling fluidized bed model was validated for the Cu-based material [19], while the model in turbulent regime was validated using Ni-, Fe,- Cu- or Mn-based materials as oxygen carrier [20-22], as well as ilmenite with solid fuels [23].

The models included the main processes affecting to the reaction of fuel gas with the oxygen carrier, such as reactor fluid dynamics, reactivity of the oxygen carrier and mechanism of the reaction. The reaction mechanism and reactivity depends on the pair gas-oxygen carrier considered, whereas the fluid dynamics is linked to the design and operating conditions of the reactor. Thus, the models were composed of two modules, the fluid dynamic and the mass balances to reacting compounds, which must be solved simultaneously due to the gas expansion of CH_4 when it is converted to CO_2 and H_2O. The oxygen carrier considered was the impregnated Cu-based oxygen carrier tested in both CLC units.

2.1. Fluid dynamics

The fluid dynamics properties of the fuel reactors affects not only to the solids distribution in the reactor, but also to the mass transference processes. Considering the impregnated oxygen carrier burning methane, the fluidization regime flow will depend on the gas velocity and the particle size of solids; see Fig. 3. Thus, low gas velocity was used in the 10 kW_{th} CLC unit to be operated in the bubbling regime. On the contrary, a higher velocity was used in the 120 kW_{th} CLC unit, which implies the fuel reactor was operated in the turbulent regime. It is interesting to note that the gas volume is increased up to a factor of 3 during CH_4 conversion to CO_2 and H_2O, and the gas velocity inside the fuel reactor was correspondingly increased.

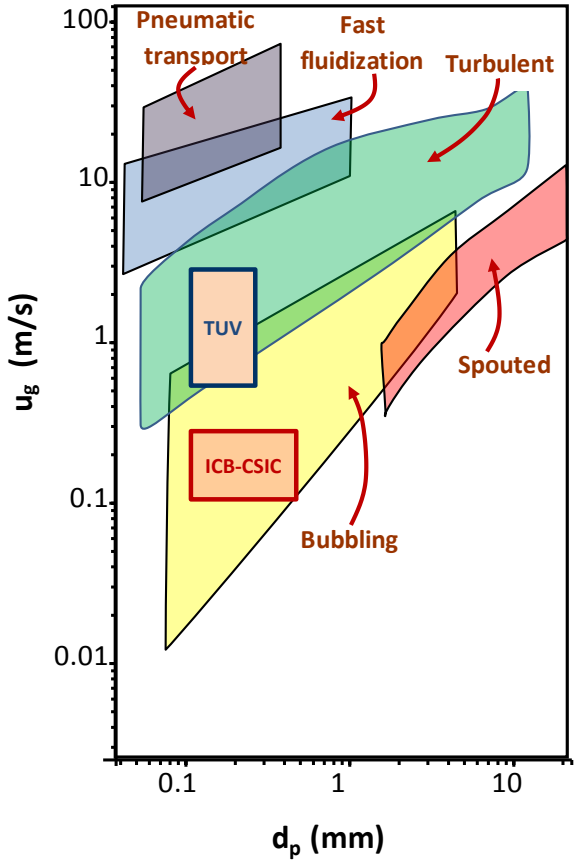

Fig. 3. Fluidization regime in the flow map for the fuel reactor burning CH_4 with the impregnated oxygen carrier used in the 10 kW_{th} unit at ICB-CSIC [10] and 120 kW_{th} unit at TUV [14]. Density of particles: 1600 kg/m^3. Adapted from [24].

The fluid dynamic model was adapted to the specific characteristics of every unit. The main equations involved in the fluid dynamic models are gathered in Table 1. More information about the specific details on the model for bubbling or turbulent regime can be found elsewhere [19,28]. Note that in some cases the same equation is valid for bubbling and turbulent regime due that both models are based on the two-phase flow theory by Kunii and Levenspiel [25], as it was adapted by Johnsson et al. for bubbling fluidized beds [26], and later revised by Pallarès and Johnsson for circulating fluidized bed [27]. Thus, as much in the bubbling as the turbulent regimes, the solids are distributed in two main regions: (1) a dense bed in the bottom part characterized by a roughly constant concentration of solids; and (2) a freeboard above the dense bed, with an exponential decay in the solids concentration with the reactor height. Both models can be considered 1.5D, i.e. are one-dimensional, but the mass exchange between bubbles and emulsion in the dense bed is considered.

In the dense bed, the gas is distributed between the emulsion, the visible bubbles and the throughflow. Gas in the emulsion is always considered at minimum fluidization conditions. Although the gas distribution is not the same for bubbling or turbulent regime, there is not significant difference in the basic structure of the model because in both cases gas in bubbles and emulsion is considered.

On the contrary, relevant differences can be found in the freeboard for bubbling or turbulent regime. Thus, in the bubbling regime only one phase for the solids in the freeboard is considered, which are in perfect mixing with solids in the dense bed. However, two phases are included in the model for the dilute region above the dense bed in the turbulent regime: (1) the splash phase formed by clusters of solids ejected from the bottom bed; and (2) the transport phase with a core-annulus structure. Both phases present an exponential decay in the solids concentration with the reactor height, but the decay constant is calculated from dedicated equations for every phase. In addition, the solids mixing is different for these phases. Solids in

the splash phase are in perfect mixing with solids in the dense bed. But the transport phase is formed by solids entrained from the dense bed, with a plug flow structure of solids rising through the core. A fraction of these solids moves laterally towards the annulus close the reactor walls, where they fall to the dense bed.

The solids distribution in the reactor is calculated by fitting the total pressure drop in the reactor from the solids concentration profile:

$$\Delta P_0 = \int_0^{H_{db}} C_{db} \mathrm{g} \mathrm{d}z + \int_{H_{db}}^{H_r} \left(C_{sp} + C_{tr} \right) \mathrm{g} \mathrm{d}z \qquad (1)$$

In this way, the upper level of the dense bed, H_{db}, is unequivocally determined.

Table 1. Equations used in the fluid dynamic model, based on [25-27].

		Bubbling FB	Circulating FB
DENSE BED			
Porosity	at minimum fluidization	$\varepsilon_{mf} = 0.586\mathrm{Ar}^{-0.029}\left(\frac{\rho_g}{\rho_p}\right)^{0.021}$	
	in the bed	$\varepsilon_{db} = (1-\delta_b)\varepsilon_{mf} + \delta_b$	
Solids	concentration	$C_{db} = \rho_s(1-\varepsilon_{db})$	
Gas	distribution	$u_0 = (1-\delta_b)u_{mf} + u_{vis} + u_{tf}$	
	minimum fluidization	$u_{mf} = \frac{\mu_g}{\rho_g d_p}\left[\sqrt{27.2^2 + 0.0408\mathrm{Ar}} - 27.2\right]$	
	visible	$u_{vis} = \psi\left(u_0 - u_{mf}(1-\delta_b)\right)$	
	throughflow	$u_{tf} = (1-\psi)\left(u_0 - u_{mf}(1-\delta_b)\right)$	
	fraction of visible	$\psi = \frac{0.26 + 0.70e^{-3300 d_p}}{(0.15 + u_g - u_{mf})^{1/3}}\left(z + 4\sqrt{A_0}\right)^{0.4}$	
Bubbles	diameter	$d_b = 0.54\left(u_0 - u_{mf}\right)^{0.4}\left(z + 4\sqrt{A_0}\right)^{0.8} g^{-0.2}$	
	volumetric fraction	$\delta_b = \frac{u_{vis}}{u_{vis} + 0.71\sqrt{g d_b}}$	
	mass transfer coefficient	$k_{be} = 4.5\left(\frac{u_{mf}}{d_b}\right) + 5.85\left(\frac{D_g^{1/2} g^{1/4}}{d_b^{5/4}}\right)$	$k_{be} = 1.631\, u_g \mathrm{Sc}^{0.37}$
FREEBOARD		**Bubbling FB**	**Circulating FB**
Gas	Terminal velocity	--	$u_t = \left(\frac{18}{\mathrm{Ar}^{2/3}} + \frac{0.59}{\mathrm{Ar}^{1/6}}\right)^{-1}\left(\frac{\rho_g^2}{\mu_g(\rho_p - \rho_g)g}\right)^{-1/3}$

Solids distribution	splash	$\frac{dC_{sp}}{dz} = -\left[\frac{2.835}{u_g}\right] C_{sp}$	$\frac{dC_{sp}}{dz} = -\left[4\frac{u_t}{u_g}\right] C_{sp}$
	transport	$C_{tr} = 0$	$\frac{\mathrm{d}C_{tr}}{\mathrm{dz}} = -\left[\frac{0.23}{u_g - u_t}\right] C_{tr}$ $C_{tr,H_{db}} = \left[\frac{131.1}{\varepsilon_{\mathrm{db}}} \rho_{\mathrm{g}} \left(\frac{\mathrm{Re}_s}{\mathrm{Ar}}\right)^{0.31}\right]_{H_{db}}$ $C_{db,H_{db}} = C_{sp,H_{db}} + C_{tr,H_{db}}$
Core diameter	$z < \{H_r - 6D_r\}$	--	$D_C = 0.87 D_r$
	$z > \{H_r - 6D_r\}$	--	$D_C = D_r - 0.0217(H_r - z)$
Solids flow		--	$F_{tr} = C_{tr} A_C (u_g - u_t)$
Gas-solid contact	efficiency	$\xi_{g-s} = 1 - 0.75\left(\frac{C_{sp} + C_{tr}}{C_{db,H_b}}\right)^{0.4}$	

2.2. Mass balances

The mass balances account for the reaction of CH_4 with the CuO present in the oxygen carrier, as expressed by the following chemical reaction:

$$CH_4 + 4\,CuO \longrightarrow CO_2 + 2\,H_2O + Cu \quad (2)$$

Differential equations for each gas, i.e. CH_4, CO_2 and H_2O in the fuel reactor shown in Table 2 are used to calculate the variation of the flow and concentration of every compound *i* in the phase *j*, $F_{j,i}$, with the reactor height. In addition to chemical reaction, $\left(-r''_{g,i}\right)_j$, main mass transference processes in the reactor are considered. Thus, both diffusion from the bulk gas phase to the external surface of the particles and diffusion of gases between bubbles and emulsion are considered. In addition, bulk transference of an excess of gases in emulsion to bubbles, F_{exc}, is considered due to the effect of gas expansion during CH_4 conversion and the limitation of gas velocity at minimum fluidization condition in the emulsion phase.

The rate of chemical reaction was included considering the kinetics parameters determined by TGA tests [19]. Kinetic parameters are shown in Table 3. In the dense bed, chemical reaction only happens in the emulsion phase. In the dilute region, reaction happens both in the splash and transport phases, but the efficiency of gas-solid contact as a function of the solids concentration is included, $\xi_{g\text{-}s}$, to consider the non-instantaneous mixing of gas and solids above the dense bed [29].

Table 2. Mass balance and reaction rate for the impregnated Cu-based oxygen carrier.

MASS BALANCES
Dense bed $\frac{dF_{e,i}}{dV} = \frac{d\left[\left(1-\delta_b\right)u_{mf}C_{e,i}\right]}{dz} = -\left(1-\delta_b\right)\sum\left(-\bar{r}''_{g,i}\right)_e - \delta_b k_{be}\left(C_{e,i}-C_{b,i}\right) - y_{e,i}\frac{dF_{exc}}{dV}$

$$\frac{dF_{b,i}}{dV} = \frac{d\left[\left(u_{vis} + u_{tf}\right)C_{b,i}\right]}{dz} = \delta_b k_{be}\left(C_{e,i} - C_{b,i}\right) + y_{e,i}\frac{dF_{exc}}{dV}$$

Freeboard

$$\frac{dF_{c,i}}{dV} = \frac{d\left[u_g C_{c,i}\right]}{dz} = -\sum \xi_{g\text{-}s}\left\{\left(-\bar{r}^{"}_{g,i}\right)_{sp} + \left(-\bar{r}^{"}_{g,i}\right)_{tr}\right\}$$

REACTION RATE

Reaction kinetics:

$$\frac{t}{\tau} = X_s \qquad \text{with} \qquad \tau = \frac{\rho_m r_g}{b\left[k_0\ e^{-E_a/R_g T}\right]C^n_{p,CH_4}}$$

The reaction rate of the oxygen-carrier, defined as dX_s/dt, was obtained by

$$-r_{s,CH_4} = \frac{dX_s}{dt} = \frac{1}{\tau}$$

Reaction considering external mass transfer in the particle:

$$\left(-r'_{g,CH_4}\right)_p = \frac{1}{b}\rho_{m,p}\left(\frac{4}{3}\pi r_p^3\right)\left[\frac{d\left(X_s(t) - \bar{X}_{s,in}\right)}{dt}\right]_{C_{p,CH_4}} = k_{g,CH_4}\left(4\pi r_p^2\right)\left(C_{bulk,CH_4} - C_{p,CH_4}\right)_z$$

Dense bed: $\mathrm{Sh} = \dfrac{k_{g,CH_4} d_p}{D_{e,CH_4}} = 2\varepsilon_{mf} + 0.117\mathrm{Ar}^{0.39}\mathrm{Sc}^{1/3}$

Freeboard: $\mathrm{Sh} = \dfrac{k_{g,CH_4} d_p}{D_{e,CH_4}} = 2\varepsilon_z + 0.69\mathrm{Re}^{1/2}\mathrm{Sc}^{1/3}$

Solids conversion distribution as a function of RTD curve, i.e. $E(t) = \dfrac{1}{t_{mr}} e^{-t/t_{mr}}$:

$$\left(1 - \bar{X}_{s,out}\right) = \int_0^{\tau_m}\left(1 - X_s(t)\right)E(t)dt \qquad \text{with} \qquad X_s(t) = \bar{X}_{s,in} + \frac{t}{\tau_m}$$

Reaction rate at position *z* in the reactor:

$$\left(-\bar{r}^{"}_{g,CH_4}\right) = \frac{\left(-\bar{r}^{"}_{s,CH_4}\right)}{b} = \frac{1}{b}\rho_{m,p}\left(1 - \varepsilon_z\right)\int_0^{t_r}\left[\frac{\mathrm{d}\left(X_s(t) - \bar{X}_{s,in}\right)}{\mathrm{d}t}\right]_{\left[C_{p,CH_4}\right]_z} E(t)\mathrm{d}t$$

being: $t_r = \tau\left(1 - \bar{X}_{s,in}\right)$

1

Table 3. Kinetic parameters for reduction of CuO in the oxygen carrier by CH_4.

			CH_4
ρ_m	molar density of CuO	mol CuO/m^3	80645
r_g	grain radius	m	$1.4 \cdot 10^{-6}$
b	Stoichiometric coefficient	mol CuO/mol CH_4	4
n	Order of the reaction	-	0.5
k_0	Pre-exponential factor	mol^{1-n} m^{3n-2} s^{-1}	480
E_a	Activation energy	kJ/mol	106

2.3. Inputs and outputs to/from the model

The models considered both the fluid dynamic of the fluidized beds at the each specific regime and the corresponding kinetics of oxygen carrier reactions. The reaction mechanism and reactivity depends on the pair gas-oxygen carrier considered, whereas the fluid dynamics is linked to the design and operating conditions of the reactor. The oxygen carrier was an impregnated Cu-based oxygen carrier, which reaction kinetics was shown in Tables 2 and 3. Table 4 shows additional characteristics of the oxygen carrier relevant for the fluid dynamic model and mass balances. A mean particle size of 0.25 mm was considered. The simplification of using a mean particle size [19], as well as neglecting diffusional effects inside the particles [30], was found to be valid for the small and narrow particle size distribution often used for oxygen carriers.

Moreover, the design and operating conditions for the 10 kW_{th} and 120 kW_{th} units are also gathered in Table 4. Some design parameters or operating conditions will be varied in this work in order to evaluate its influence on the CLC performance. Specifically, the reactor height was increased in some cases in order to maintain a fully developed profile of solids in the freeboard. But the following operating conditions will be maintained constant over all this work, namely: temperature, total pressure, fuel flow, oxygen carrier to fuel ratio and solids conversion in the air reactor. In this sense, it is assumed that the oxygen carrier is not fully

oxidized in the air reactor, which is a realistic condition when the minimum amount of solids in the whole CLC unit is determined [31].

Table 4. Geometric parameters and operational conditions for the 10 kW_{th} and 120 kW_{th} CLC units.

	Symbol	Units	10 kW unit	120 kW unit
Reactor geometry				
Height(1)	H_r	m	1.2	3.0
Diameter(1)	D_r	m	0.10	0.16
Specific cross section area(1)	S_{MW}	m^2/MW_{th}	1.16	0.20
Number of nozzles(1)	N_{nz}	-	68	3
Operational conditions				
Temperature	T	K	1073	1073
Pressure at the outlet	P	Pa	101325	101325
Thermal power	P_{th}	kW	8	100
Inlet fuel flow	Q_f	Nm^3/h	0.8	10
Oxygen carrier to fuel ratio	ϕ	-	2	2
Circulation rate of solids	Q_s	kg/h	230	2850
Pressure drop(1)	ΔP	Pa	1000	5900
Inventory of solids in the fuel reactor(1)	m_s	kg	0.94	12.0
Specific Inventory in the fuel reactor(1)	m_s^*	kg/MW_{th}	120	120
Inlet gas velocity(1)	u_g	m/s	0.1	0.52
Solids conversion in the air reactor	$\bar{X}_{o,AR}$	-	0.7	0.7
Oxygen carrier characteristics				
CuO mass fraction in the oxygen carrier	x_{CuO}	-	0.1	0.1
Mean particle diameter(1)	d_p	mm	0.25	0.25
Density of particles	ρ_p	kg/m^3	1600	1600

(1) For reference conditions

The main outputs of the model were (1) the fluid dynamics structure of the reactor, e.g. height of the dense region and profiles of concentration and flow of solids in the dilute region; (2) the axial profiles of gas composition and flows (CH_4, CO_2 and H_2O); (3) the axial profiles of average conversion for the oxygen carrier; and (4) the gas composition and solids flow in the upper reactor exit.

From these outputs, the performance of the CLC system was assessed by calculating the CH_4 conversion in the fuel reactor, X_{CH_4}.

$$X_{CH_4} = \frac{F_{in,CH_4} - F_{out,CH_4}}{F_{in,CH_4}} \quad (3)$$

3. Results

The CLC models were used to analyse and to optimize the performance of the CLC process under different fluid dynamic conditions. Thus, several issues affecting to the fluid dynamic, such as solids inventory, gas velocity or particle size, were evaluated with both models, i.e. model for the fuel reactor either at bubbling or turbulent regimes. The fluidization regime influences to the mass transference processes and solids distribution in the fuel reactor, which eventually would affect to the amount of solids required to fully convert the fuel.

Now, a brief discussion about the relevance of the fluid dynamic regime in the methane conversion is shown by evaluating the axial profiles of gases and solids in the reactor; see Fig. 4. Reference in both the 10 and 120 kW_{th} units were assumed; see Table 4. The separation of the dense bed and the dilute region can be easily observed. For the same specific solids inventory (120 kg/MW_{th}), the height of the dense bed is higher in the turbulent regime than in the bubbling regime due to the lower specific cross section area for the turbulent case. In the bubbling regime, the dense bed is characterised by a roughly constant fraction of solids, while the solids concentration slightly decreases in the turbulent regime. In both cases, the solids concentration strongly decreases in the freeboard. More interesting is the fact that methane is slowly converted in the dense bed because the chemical reaction is restricted by the diffusion of methane from the bubbles to the emulsion phase, where reaction with the oxygen carrier happens. Nevertheless, a relevant fraction of methane is converted in the dense bed; but methane is converted faster in the freeboard because an improved contact between gas and

solids is found in this region. Thus, the conversion in the freeboard is a key factor in order to achieve high combustion efficiency.

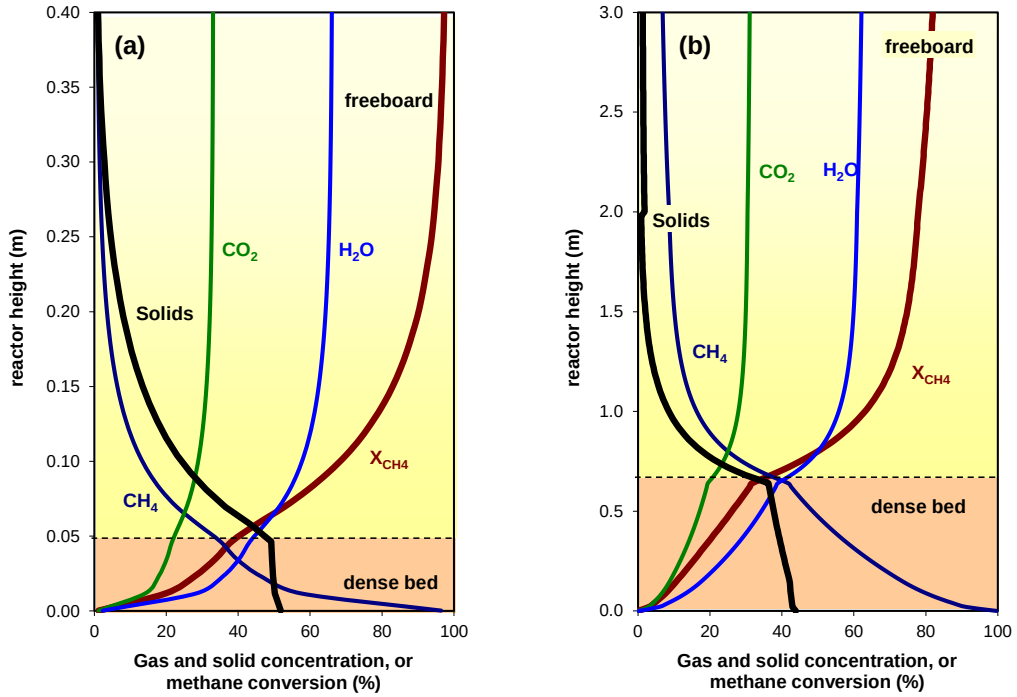

Fig. 4. Longitudinal profiles of gas and solids concentration in the fuel-reactor. (a) Bubbling regime; (b) Turbulent regime.

Following, results from each model are discussed independently, and eventually the performance of a CLC unit under different regimes is compared.

3.1. Fuel reactor in the bubbling regime

A key parameter for the design of a CLC system is the solids inventory in the fuel reactor, which is linked and dependent on the reactivity of the oxygen carrier and fluid dynamics of the reactor. Considering the reference conditions shown in Table 4, the model was used to predict the methane conversion as a function of the solids inventory in the fuel reactor; see Fig. 5. High methane conversion is achieved even with solids inventory values as low as 100 kg/MW_{th} because the high reactivity of the Cu-based oxygen carrier. The different solids inventory mainly affect to the solids present in the dense bed. Thus, the conversion of

methane in the dense bed decreases as the solids inventory decreases. But the solids in the freeboard are not capable to fully convert the methane at least that the total solids inventory was higher than 225 kg/MW_{th}, which means that the fuel conversion in the dense bed must be higher than 57 %. Nevertheless, solids in the freeboard are essential in order to get complete conversion due to solids in the upper part of the dense bed are less effective burning methane.

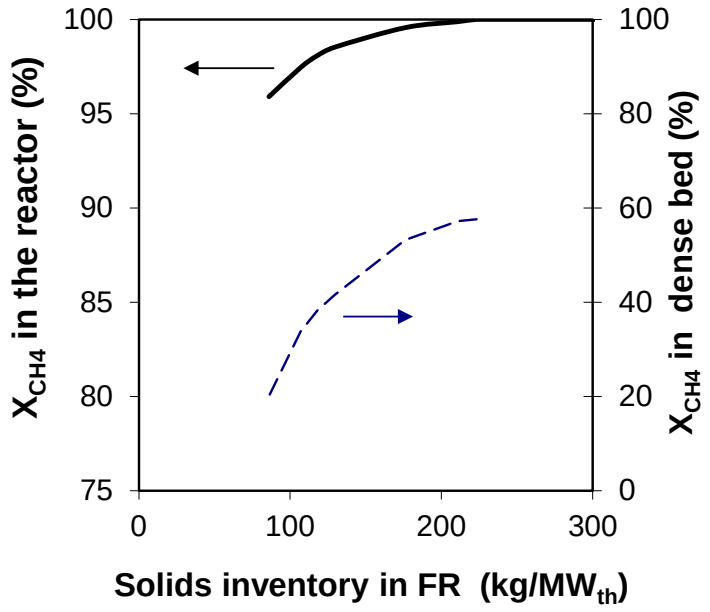

Fig. 5. Methane conversion in the whole fuel reactor and in the upper limit of the dense bed as a function of the solids inventory in the fuel reactor for the bubbling regime (BFB). S_{MW} = 1.15 m^2/MW_{th}; d_p = 0.25 mm.

For the subsequent analysis, a value of 120 kg/MW_{th} was selected, where incomplete conversion of methane is predicted; thus the effect of other factors on the methane conversion could be evaluated.

The effect of the mean particle size of solids on the methane conversion is shown in Fig. 6. Clearly, the methane conversion can be improved by increasing the particle size of the oxygen carrier, thus achieving the complete combustion of methane with 120 kg/MW_{th} of solids with a mean particle size of 0.5 mm. The ultimate reason for this behaviour is found in the fluid

dynamic characteristics of a bubbling fluidized bed. It was assumed that the fluidizing gas, which is the fuel in CLC, is shared between the emulsion and bubbles, with gas in emulsion maintained at minimum fluidization velocity. But the minimum fluidization velocity increases from 0.0034 to 0.0845 m/s when the particle size increased from 0.1 to 0.5 mm. Consequently, the fraction of gas going through the emulsion increased from 3 % to 87 %; see Fig. 6. Note that gas in bubbles must diffuse to the emulsion phase to react with the oxygen carrier, but gas in the emulsion has a good contact with the oxygen carrier particles and can be quickly converted. In addition, the mass transfer coefficient between bubbles and emulsion, k_{be}, also increases with the particle size of solids. All this benefits the methane conversion as the particle size is increased.

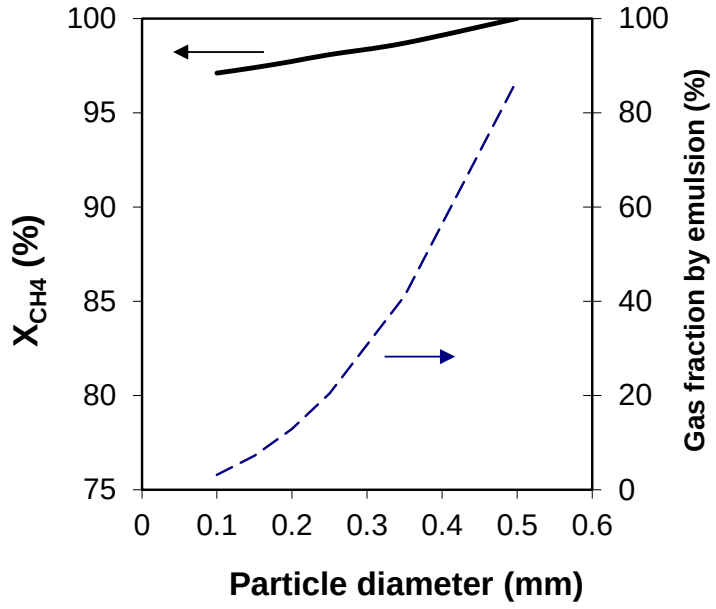

Fig. 6. Methane conversion predicted by the model in bubbling regime (BFB) as a function of the particle size of the oxygen carrier. The fraction of gas initially flowing through the emulsion is also shown. S_{MW} = 1.15 m^2/MW_{th}; ΔP = 1000 Pa (m_s^* = 120 kg/MW_{th}).

Although the benefit of using a higher particle size to improve the methane conversion in the fuel reactor was shown, in this discussion is necessary to take into account the fluid dynamic

of the air reactor, which will be also affected by the particle size of the oxygen carrier. The air reactor would be designed as a circulating fluidized bed in order to support the solids circulation rate required by the CLC process. In this sense, considering that the terminal velocity also increases significantly with the particle size, the entrainment of solids from the air reactor would be harder. Thus, the terminal velocity for the oxygen carrier particle size of 0.5 mm is estimated to be u_t = 4 m/s, which would require an extremely high velocity in the air reactor to achieve the required solids flow from the air reactor to the fuel reactor. A more realistic condition can be found for a mean particle size of d_p = 0.25 mm, with u_t = 1.3 m/s.

Another operating condition affecting the fluid dynamic of the fuel reactor is the gas velocity. Assuming the fuel as pure CH_4 in CLC, the gas velocity determines the cross section area of the fuel reactor per thermal power. Simulations with the model were done by varying the gas flow in the fuel reactor, i.e. the thermal power. In order to properly evaluate the effect of the gas velocity on the methane conversion, the specific solids inventory in the reactor was unchanged; assuming a value of 120 kg/MW_{th}. Consistently, the pressure drop in the reactor was fitted as required depending on the fuel flow. Simulation results are presented in Fig. 7, where the evolution of the methane conversion with the cross section is shown. The gas velocity changed with the cross section per thermal power from 0.1 to 0.55 m/s. In addition, an analysis to the profiles of both solids concentration and methane conversion in the reactor is done to better observe the effect of the cross section; see Fig. 8.

At reference conditions, the cross section area is high, namely 1 m^2/MW_{th}, which implies a low gas velocity and high CH_4 conversion, X_{CH_4} =98%. Then, a decrease of the methane conversion is predicted when the reactor section decreases. On the one hand, the gas fraction in bubbles increases as the cross section area decreases and the gas velocity increases; in a similar way that it was shown above when the particle size decreased. In addition, solids in the dense bed became less effective converting methane due to the gas transference between

bubbles and emulsion is harder, i.e. the bubble diameter increases and the mass transfer coefficient k_{be} decreases. As a result, a lower conversion of methane is achieved in the dense bed (see Fig. 8). On the other hand, the higher gas velocity promotes the evolution of solids in the freeboard, which are more effective converting methane than solids in the dense bed. However, the taller dense bed makes that the fraction of solids in this region increases as the cross section decreases. Consequently, the fraction of solids in the freeboard decreases with the cross section decrease, which eventually induces a lower methane conversion in the fuel reactor.

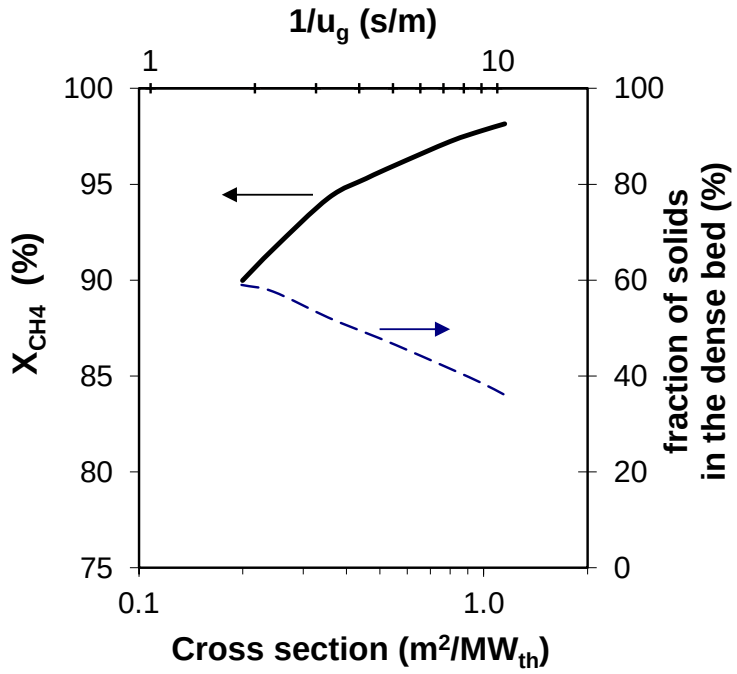

Fig. 7. Methane conversion predicted by the model in the bubbling regime (BFB) as a function of the specific cross section area, S_{MW}. The fraction of solids remaining in the dense bed is also shown. d_p = 0.25 mm; m_s^* = 120 kg/MW$_{th}$.

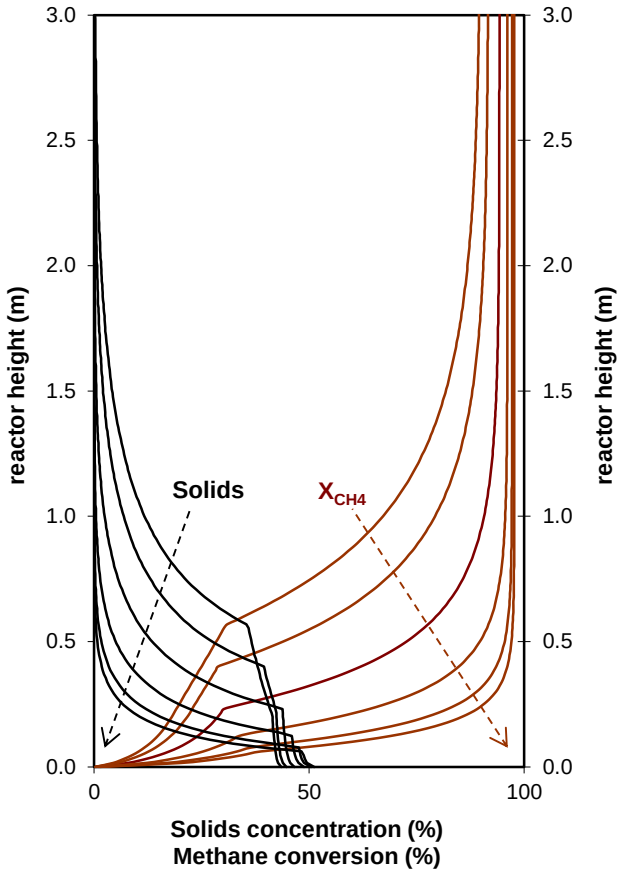

Fig. 8. Axial profiles of the solids concentration and the methane conversion as the cross section area increases, considering the following list: S_{MW} (m^2/MW_{th}) = 0.20<0.25<0.36<0.56<0.8<1. d_p = 0.25 mm; m_s^* = 120 kg/MW_{th}.

3.2. Fuel reactor in the turbulent regime

First, a sensitivity analysis was done to the solids inventory in fuel reactor by changing the pressure drop in the reactor. Fig. 9 shows the methane conversion predicted by the model as a function of the specific solids inventory in the fuel reactor. Additional solids go mainly to the dense bed, but distribution of solids in the dilute region was barely affected. Due to important limitations in the gas transference between bubbles and emulsion in the turbulent regime, the methane conversion in the dense bed is slower than in the bubbling regime; see Fig. 4. This fact implies that it is necessary a relevant amount of additional oxygen carrier to reach high

values of methane conversion. Therefore, the specific solids inventory in the fuel reactor to achieve the complete conversion of methane is higher in the turbulent regime, namely 600 kg/MW_{th} aprox. At this condition, the methane converted in the dense bed is about 75 %, which means that the capability of the freeboard converting methane is low with the particle size considered (0.25 mm). At reference conditions, the gas velocity in the freeboard barely exceeds the terminal velocity of the particles, which makes that the amount of solids in the dilute region was low.

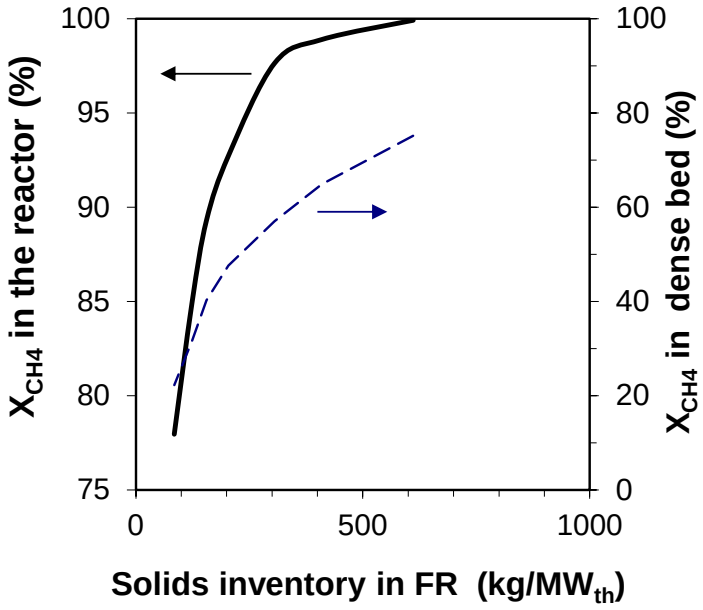

Fig. 9. Methane conversion in the whole fuel reactor and in the upper limit of the dense bed as a function of the solids inventory in the fuel reactor for the turbulent regime (CFB). S_{MW} = 0.2 m^2/MW_{th}; d_p = 0.25 mm.

Then, a sensitivity analysis was also done to the particle size of the oxygen carrier in the turbulent regime. The model predicts a higher fraction of solids is in the dilute region as the particle size decreases, increasing the amount of particles both in the cluster and transport phases. In fact, the transport phase appears for solids with a particle size lower than 0.25 mm, condition required to achieve a gas velocity in the upper surface of the dense bed higher than

the terminal velocity of solids. The change on the distribution of solids with different particle size affected to the methane conversion; see Fig. 10. The fuel conversion is higher when lower particle sizes are used due to the improved gas-solid contact in the dilute region compared to the dense bed. Therefore, complete combustion of the fuel with 120 kg/MW_{th} in the fuel reactor was predicted when the particle size of the oxygen carrier was lower than 0.14 mm. This behaviour is opposite to those observed in the bubbling regime; see Fig. 6. Thus, the particle size of the oxygen carrier must be customized considering the fluidization regime of the fuel reactor. While the suitable mean particle size was 0.14 mm in the turbulent regime, 0.5 mm was required in the bubbling regime to achieve full methane conversion with 120 kg/MW_{th}.

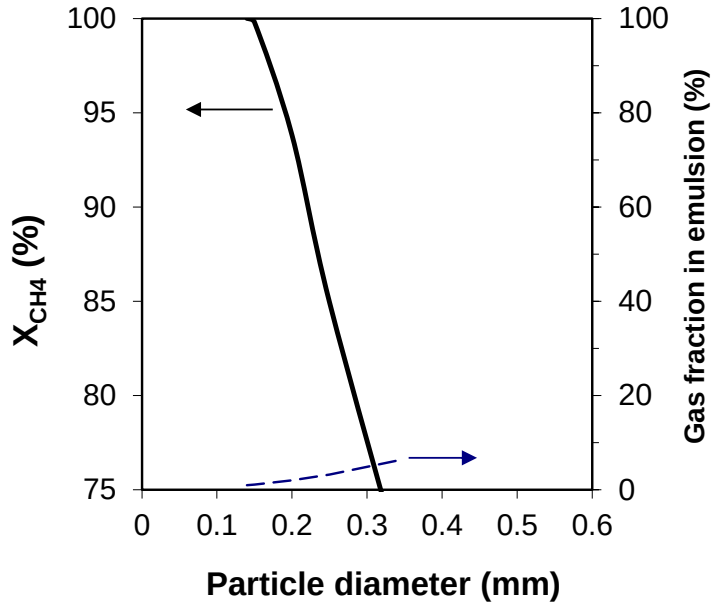

Fig. 10. Methane conversion predicted by the model in turbulent regime (CFB) as a function of the particle size of the oxygen carrier. The fraction of gas initially flowing through the emulsion is also shown. S_{MW} = 0.2 m^2/MW_{th}; ΔP = 5900 Pa (m_s^* = 120 kg/MW_{th}).

The presence of solids in the dilute region can also be improved by increasing the gas velocity, which can be achieved by increasing the fuel flow; thus, the specific section of the

reactor per thermal power is decreasing. Considering the high effect of the particle size of solids on the methane conversion in the fuel reactor, Fig. 11 shows the results predicted by the model for two particle sizes (0.15 and 0.25 mm) assuming a specific solids inventory of 120 kg/MW_{th} in all cases. For the higher particle size, an increase in the methane conversion is clearly observed as the specific cross section area is decreased. Consequently, the gas velocity is increased, which improves the methane conversion both in the dilute region, which benefits the fuel converted in the whole reactor. However, this also affects to the required pressure drop in the reactor to maintain the specific solids inventory in the reactor. Thus, the pressure drop would be 60 kPa assuming a specific section of 0.02 m^2/MW_{th}, and even in this case complete combustion of methane is not achieved with a particle size of 0.25 mm.

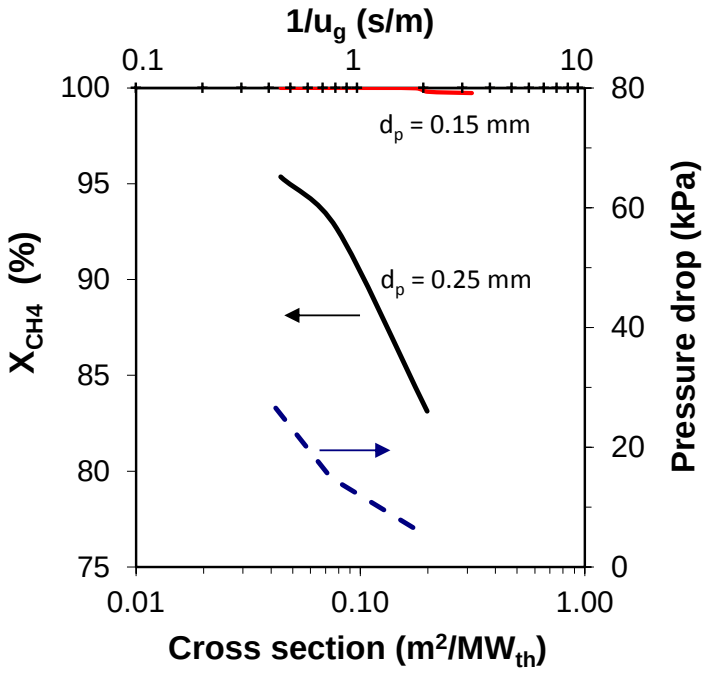

Fig. 11. Methane conversion predicted by the model in the turbulent regime (CFB) as a function of the specific cross section area, S_{MW}. The pressure drop in the reactor is also shown. d_p = 0.15 or 0.25 mm; m_s^* = 120 kg/MW_{th}.

Then, the sensitivity analysis was done with a suitable particle size of 0.15 mm. In this case, the methane conversion was complete for values of the specific cross section lower than 0.18 m^2/MW_{th}. At this condition, the pressure drop in the fuel reactor would be 6.6 kPa. Again, the lower terminal velocity for smaller particles is the main reason of this behaviour. So, the distribution of solids in the reactor changes as the particle size decreases, transferring solids from the low effective dense bed to the dilute region, which is more effective burning methane when there are enough amount of solids.

4. Practical implications on CLC design

A key parameter for the design of a CLC unit is the solids inventory in the reactors. Too low solids inventory would not allow the complete conversion of the fuel, while a high excess of solids would negatively affect to the energetic efficiency of the plant due to a high pressure drop in the reactor [32,33]. Now, the models were used to determine the minimum solids inventory required to achieve complete methane conversion. In addition, it was determined that the gas transference between the bubble and emulsion is a limiting process to convert the fuel in the dense region. This process is determined by the bubble size, which depends on the reactor geometry. In order to cover a broad context, results were obtained limiting the growing of bubbles at different sizes (d_b = 0.05, 0.1 and 0.15 m). Also unlimited growing of the bubbles was considered.

Fig. 12 shows the required solids inventory to achieve complete conversion of methane both in bubbling and turbulent regime. Considering a particle size of 0.25 mm, fluidization in the bubbling regime requires the use of low amount of solids in the fuel reactor with high cross section per thermal power regardless of the limit imposed on the growth of bubbles. However, as the cross section decreases, the increase in the required amount of solids is stronger as the bubbles are bigger. In fact, the solids inventory become very high (>1000 $kg(MW_{th})$ when no

limitation in the growing of the bubbles is considered. This fact is related to the taller dense zone as the cross section decreases, which allows bigger bubbles in the dense zone. Consequently, the conversion of methane is hampered in the dense zone. If low solids inventory is desired, the growing of the bubbles should be limited in any way. Otherwise, cross section area values about 1 m^2/MW_{th} should be used. If we analyse the curve obtained for a maximum bubble size of 0.05 m, we observe that the minimum solids inventory reaches a maximum in the central region, which corresponds to the conditions where methane was more difficult to convert. In this case, solids in the freeboard are not promoted due to the low gas velocity. But the solids inventory decreases again when the cross section decreases below 0.5 m^2/MW_{th} because the gas velocity become high enough to support a high concentration of solids in the freeboard, which is more efficient converting methane than solids in the dense zone. In the bubbling regime, minimum values of the required solids inventory is about 250 kg/MW_{th}.

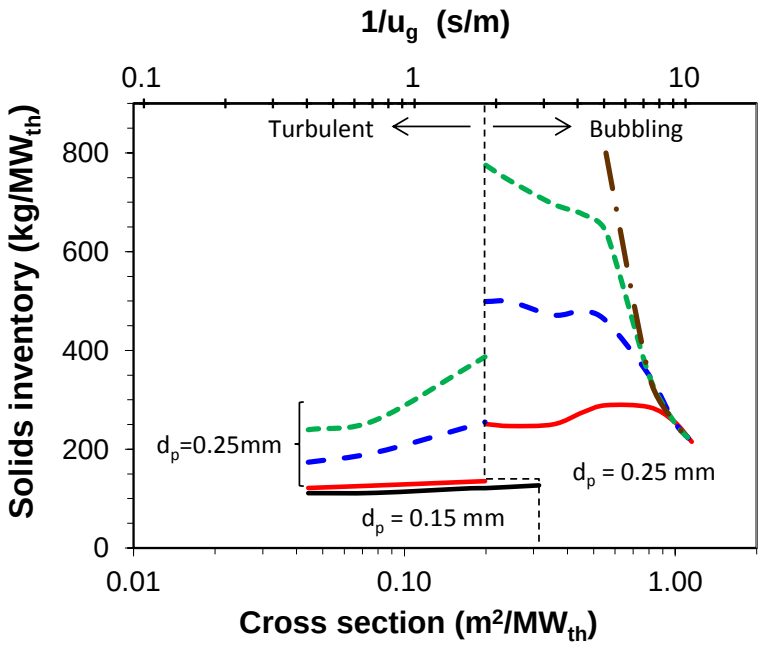

Fig. 12. Minimum solids inventory in the fuel reactor, both in bubbling and turbulent regimes, to achieve full fuel conversion as a function of the specific cross section, S_{MW}. Maximum value of the bubble size: 0.05 m (——); 0.1 m (– – –); 0.15 m (- - - -); unlimited (— · —).

The theoretical model shows that the fluidization regime changes from bubbling to turbulent when the cross section decreases from 0.2 m^2/MW, corresponding to a gas velocity at the fuel reactor inlet of 0.52 m/s. At this point, the transport phase is developed and the freeboard is characterized by a core-annulus structure. An abrupt change in the minimum solids inventory is observed in the transition line from bubbling to turbulent regime. Thus, the solids inventory in the turbulent regime is lower than in the bubbling regime, which is mainly due to the existence of the transport phase and different decay constant for either bubbling or turbulent regime; see Table 1. High confidence on the model results can be considered for similar conditions to those used in validation works [19-23]. These conditions include the following interval of cross section values: 0.6-1.3 m^2/MW_{th} for bubbling regime and 0.14-0.2 m^2/MW_{th} for turbulent regime. We have not found experimental results obtained in the bubbling regime with lower cross section values in order to validate our model at these conditions. Therefore, we must be cautious in the analysis of the results obtained with cross section between 0.2-0.6 m^2/MW_{th} in the bubbling regime. However, results are sound, and relevant conclusions can be extracted from this work, namely it is highlighted the solids inventory can be maintained at low values if the growing of the bubble size is limited in any way. These results encourage the design of future experiments at these conditions in order to validate the model predictions.

In the turbulent regime, it is highly relevant that low solids inventory is predicted when limited growing of bubbles is considered, e.g. d_b = 0.05-0.1 m. However, more relevant are the results obtained if a proper particle size was selected for this fluidization regime, i.e. smaller particles than in the bubbling regime. In this case, the lower terminal velocity of the solids as the particle size decreases (0.5 and 1.3 m/s for particle size of 0.15 and 0.25 mm, respectively) influences on the solids distribution in the reactor, which eventually improves the methane conversion; see Section 3.2. The minimum solids inventory with particles of 0.15

mm is 125 kg/MW_{th}. In addition, results with the lowest particle size were not sensible to the growing of the bubbles, and similar results were obtained regardless the imposed limit to the bubble size. This effect was because the low amount of solids in the dense bed and the high relevance of methane conversion by solids in the dilute region. The gap in the minimum solids inventory with different particle sizes decreases as the cross section decreases. This fact is due to the high increase in the gas velocity, which makes less relevant the difference in the terminal velocity. Nevertheless, the design and operation of the fuel reactor at these conditions would be hampered because the high pressure drop required in the reactor.

For a more complete view of the suitable operating conditions in the fuel reactor, the pressure drop in the reactor as a function of the minimum solids inventory was also evaluated. Fig. 13 shows the relation between the specific cross section area, S_{MW}, and the gas velocity and pressure drop depending on the solids inventory in the fuel reactor. An interval of cross section area for the fuel reactor can be selected depending on the desired gas velocity. Thus, the operation of bubbling regime with particles size of 0.25 mm is limited to cross section area higher than 0.2 m^2/MW_{th} and inlet gas velocities lower than 0.6 m/s. The suitability of the bubbling regime for cross section area lower than 0.8 m^2/MW_{th} is limited to conditions at which bubbles are of small size; here results with a maximum bubble size of 0.05 m are presented. No limitation in the bubble size can be considered for bigger values of the cross section. The required pressure drop also decreases when the cross section increases, and it is maintained below 12 kPa. A pressure drop as low as 2.6 kPa is determined assuming a cross section area of 1 m^2/MW_{th}.

For a circulating fluidized bed (CFB), a particle size of 0.15 mm was selected. In order to hava a proper dilute region with a transport phase, the specific cross section must be lower than 0.3 m^2/MW_{th} in order to the inlet gas velocity was higher than 0.4 m/s. As the cross section decreases, the solids inventory is maintained slightly above 100 kg/MW_{th}, but the

pressure drop increases significantly. Thus, the operation with cross section values lower than 0.04 m^2/MW_{th} could be problematic due to the pressure drop values above 30 kPa would be required. If the pressure drop is desired to be stretched below 10 kPa, the cross section area must be above 0.11 m^2/MW_{th}. A suitable condition would be the selection of solids with a mean particle size of 0.15 mm, designing the fuel reactor with 0.2 m^2/MW_{th}, which fix the pressure drop in 6 kPa and the inlet gas velocity in 0.55 m/s. Considering a reactor height of 10 m to have a fully developed dilute region, the volume of the fuel reactor chamber would be 2 m^3/MW_{th}. The same volume can be determined for a bubbling fluidized bed 2 m tall, which also would be feasible.

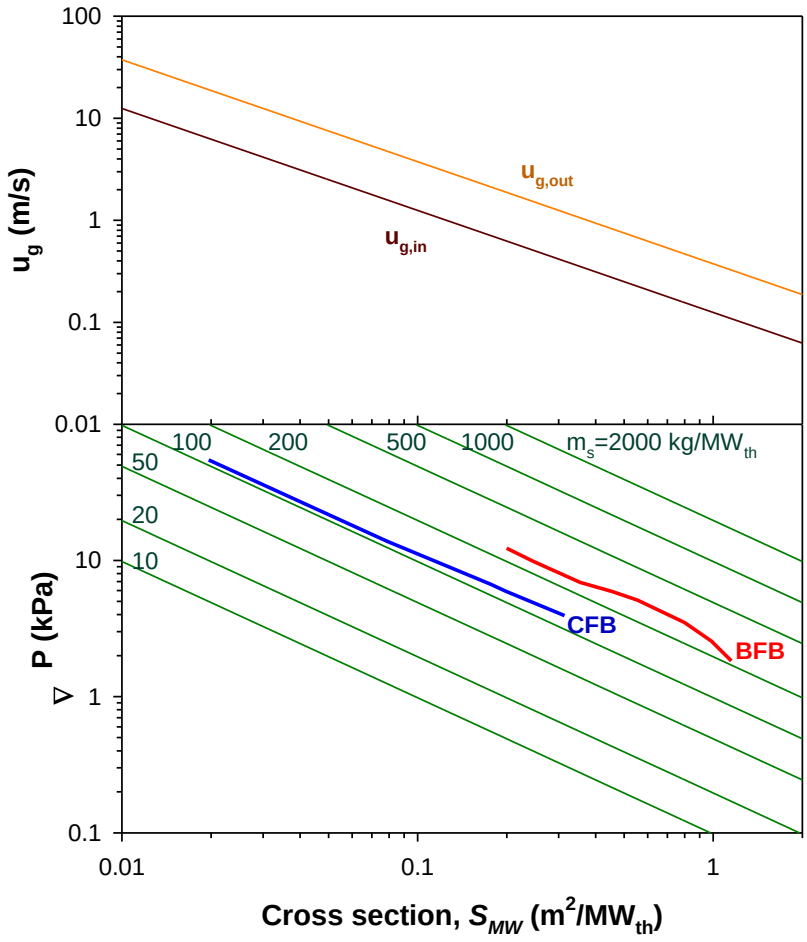

Fig. 13. Relation between design parameters (specific cross section, S_{MW}, and solids inventory, m_s) and operating conditions (u_g, ΔP) for the design of a CLC unit burning CH_4

considering the fuel reactor being either a bubbling fluidized bed (BFB) with d_p = 0.25 mm or a circulating fluidized bed (CFB) with d_p = 0.15 mm.

The values of solids inventory determined for the Cu-based oxygen carrier is among the lowest considering the state of the art of the oxygen carrier development [2]. Note that the solids inventory in the boiler is a key parameter for the design and proper operation of the fluidized bed. Should commercial experience on fluidized bed boilers is used the up-scaling of CLC would be boosted. For example, the 252 MW_{th} CFB Combustor at Duisburg operates with solids inventory about 200 kg/MW_{th} [34], which is in line with solids inventory values required for CLC using the Cu-based oxygen carrier. In the bubbling regime, the amount of solids in the reactor would be higher than in the circulating bed: 250 vs. 125 kg/MW_{th}, but the pressure drop would be lower (2.6 vs. 6 kPa). In addition, higher oxygen carrier losses would be expected in the CFB configuration because: (1) the mecanical strength of the oxygen carriers usually is lower for smaller particle size [35,36]; (2) the cyclone could not recover all the particles, especially fines produced by attrition. All these factors should be taken into account in the optimum design of the fuel reactor.

5. Conclusions

Methane conversion in a CLC unit with a highly reactive Cu-based oxygen carrier was predicted by modelling the fuel reactor in both the bubbling and turbulent regimes. The solids distribution and the efficiency of solids burning methane both in the dense bed and in the freeboard were dependent on the fluidization regime. Therefore, the fluid dynamic characteristics of the fuel reactor must be considered for a proper design of a CLC unit.

Considering conditions in existing CLC units, 10 kW_{th} at ICB-CSIC and 120 kW_{th} at TUV with a particle size of 0.25 mm in both cases, the minimum solids inventory to achieve full

methane conversion was determined to be 225 or 600 kg/MW_{th} for the bubbling and turbulent regime, respectively. A lower solids inventory is required in the turbulent regime when the particle size was decreased to 0.15 mm.

For design purposes, big particles (0.25 mm) and low gas velocity (0.1 m/s), with cross section area of 1 m^2/MW_{th}, is recommended for the bubbling regime in order to minimize the required amount of solids to 250 kg/MW_{th}. If the cross section per thermal power was lower, the growing of the bubbles should be restricted.

On the contrary, lower particle size (0.15 mm) and higher gas velocity is required for the turbulent regime, but limited to 0.5-0.6 m/s to avoid high excess in the pressure drop. In this case, the minimum solids inventory was determined to be 125 kg/MW_{th} assuming a cross section of 0.2 m^2/MW_{th}.

ACKNOWLEDGMENTS

This paper was supported by the European Commission Seventh Framework Program under the grant agreement N° 608571 (Project acronym SUCCESS), and by the Spanish Ministry of Economy, Industry and Competitiveness (MINECO Projects: ENE2014-56857-R and ENE2016-77982-R) and the European Union FEDER funds.

Nomenclature

A_0	area of the gas-distributor per nozzle, m^2 per nozzle
A_C	core section, m^2
Ar	Archimedes number
b	stoichiometric factor in the reduction reaction, mol of solids reacting (mol of gas)$^{-1}$
$C_{b,i}$	concentration of gas i in the bubbles, mol m^{-3}
$C_{bulk,i}$	concentration of gas i in the bulk phase, mol m^{-3}
C_{db}	concentration of solids in dense bed, kg m^{-3}
$C_{e,i}$	concentration of gas i in the emulsion, mol m^{-3}
$C_{p,i}$	concentration of gas i in the particle, mol m^{-3}
C_{sp}	concentration of solids in splash region, kg m^{-3}
C_{tr}	concentration of solids in transport region, kg m^{-3}
d_b	diameter of bubble, m
d_p	diameter of particle, m
D_C	diameter of core, m
$D_{e,i}$	effective diffusivity of gas i, m^2 s^{-1}
D_g	diffusivity of gas, m^2 s^{-1}
D_r	diameter of reactor, m
E_a	activation energy, J mol^{-1}
$E(t)$	function of the distribution of residence time
$F_{b,i}$	molar flow of gas i in the bubbles, mol s^{-1}

1 $F_{c,i}$ molar flow of gas *i* in the core, mol s^{-1}

2 $F_{e,i}$ molar flow of gas *i* in the emulsion, mol s^{-1}

3 F_{exc} molar flow in excess in the emulsion being transferred to bubbles, mol s^{-1}

4 F_{in,CH_4} inlet molar flow of methane to the reactor, mol s^{-1}

5 F_{out,CH_4} outlet molar flow of methane from the reactor, mol s^{-1}

6 F_{tr} flow of solids in the transport phase, kg s^{-1}

7 g acceleration due to gravity, m^2 s^{-1}

8 H_{db} deep of the dense bed, m

9 H_r reactor height, m

10 k_0 preexponential factor of the rate constant, mol^{1-n} m^{3n-2} s^{-1}

11 k_{be} coefficient for gas exchange between bubble and emulsion, s^{-1}

12 $k_{g,i}$ coefficient of mass transfer of gas *i* around the particle, m s^{-1}

13 m_s solids inventory in the reactor, kg

14 m_s^* specific inventory of solids in the reactor, kg MW_{th}^{-1}

15 n order of reaction

16 N_{nz} number of nozzles in the distributor plate

17 P pressure, Pa

18 r_g grain radius, m

19 r_p particle radius, m

20 $\left(-r''_{g,i}\right)_j$ reaction rate of gas *i* in the phase *j*, mol m^{-3} s^{-1}

$\left(-r_{s,i}\right)$ reaction rate of the oxygen carrier with gas *i*, s^{-1}

$\left(-r'_{s,i}\right)_p$ reaction rate of the oxygen carrier with gas *i* in the particle, mol s^{-1}

$\left(-r''_{s,i}\right)$ reaction rate of solid with gas *i*, mol m^{-3} s^{-1}

R_g constant for the ideal gases, J mol^{-1} K^{-1}

Re Reynolds number

S_{MW} cross section area of the reactor per thermal power, m^2 MW_{th}^{-1}

Sc Schmidt number

Sh Sherwood number

t time, s

t_{mr} mean residence time, s

t_r reaction time from conversion of the carrier $X_s = 0$ until the maximum variation in the conversion, s

T temperature, K

u_0 velocity of the total gas flow, m s^{-1}

u_g gas velocity, m s^{-1}

u_{mf} velocity of minimum fluidization, m s^{-1}

u_t terminal velocity, m s^{-1}

u_{tf} velocity of the gas throughflow, m s^{-1}

u_{vis} visible velocity of a bubble, m s^{-1}

V volume, m^3

x_i mass fraction of the compound i

X_{CH_4} conversion of methane

$\bar{X}_{o,AR}$ mean conversion of particles for oxidation reaction reached in the air-reactor

X_s conversion of the oxygen-carrier for the reduction reaction

$\bar{X}_{s,in}$ mean conversion of particles at the fuel reactor inlet

$\bar{X}_{s,out}$ mean conversion of particles at the fuel reactor outlet

$y_{e,i}$ mole fraction of gas *i* in the emulsion

z axial position in the reactor, m

Greek symbols

δ_b fraction of bubble in the dense bed

ΔP_0 pressure drop in the reactor, Pa

ε_{db} porosity at the dense bed

ε_{mf} porosity at minimum fluidization

ε_z porosity at the height *z*

ϕ ratio of oxygen-carrier to fuel

μ_g viscosity of fluidizing gas, kg m^{-1} s^{-1}

ρ_g density of gas, kg m^{-3}

ρ_m molar density, mol m^{-3}

$\rho_{m,p}$ molar density of active compound of the oxygen carrier in the particle, mol m^{-3}

ρ_p density of particle, kg m^{-3}

ρ_s density of solid, kg m^{-3}

τ time for complete conversion of the carrier, s

τ_m mean time for complete reaction of the carrier, s

$\xi_{g\text{-}s}$ efficiency of contact between gas and solids in the freeboard

Ψ ratio of the visible bubble flow to the total flow through the bubbles

6. References

[1] F. Petrakopoulou, G. Tsatsaronis. Can Carbon Dioxide Capture and Storage from Power Plants Reduce the Environmental Impact of Electricity Generation? Energy Fuels 28 (2014) 5327-5338.

[2] J. Adanez, A. Abad, F. García-Labiano, P. Gayán, L.F. de Diego. Progress in Chemical-Looping Combustion and Reforming technologies. Prog. Energ. Combust. Sci. 38 (2012) 215-282.

[3] A. Cabello, P. Gayán, A. Abad, L.F. de Diego, F. García-Labiano, M.T. Izquierdo, A. Scullard, G. Williams, J. Adánez. Long-lasting Cu-based Oxygen Carrier Material for Industrial Scale in Chemical Looping Combustion. Int. J. Greenhouse Gas Control 52 (2016) 120-129.

[4] L.F. de Diego, P. Gayán, F. García-Labiano, J. Celaya, A. Abad, J. Adánez. Impregnated CuO/Al_2O_3 Oxygen Carriers for Chemical-Looping Combustion: Avoiding Fluidized Bed Agglomeration. Energy Fuels 19 (2005) 1850-1856.

[5] C.R. Forero, P. Gayán, L.F. de Diego, A. Abad, F. García-Labiano, J. Adánez. Syngas combustion in a 500 W_{th} Chemical-Looping Combustion system using an impregnated Cu-based oxygen carrier. Fuel Process. Technol. 90 (2009) 1471-1479.

[6] P. Gayán, C.R. Forero, L.F. de Diego, A. Abad, F. García-Labiano, J. Adánez. Effect of gas composition in Chemical-Looping Combustion with copper-based oxygen carriers: Fate of light hydrocarbons. Int. J. Greenhouse Gas Control 4 (2010) 13-22.

[7] C.R. Forero, P. Gayán, F. García-Labiano, L.F. de Diego, A. Abad, J. Adánez. Effect of gas composition in Chemical-Looping Combustion with copper-based oxygen carriers: Fate of sulphur. Int. J. Greenhouse Gas Control 4 (2010) 762-770.

[8] P. Gayán, C.R. Forero, A. Abad, L.F. de Diego, F. García-Labiano, J. Adánez. Effect of Support on the Behavior of Cu-Based Oxygen Carriers during Long-Term CLC Operation at Temperatures above 1073 K. Energy Fuels 25 (2011) 1316-1326.

[9] C.R. Forero, P. Gayán, F. García-Labiano, L.F. de Diego, A. Abad, J. Adánez. High temperature behaviour of a $CuO/\gamma Al_2O_3$ oxygen carrier for chemical-looping combustion. Int. J. Greenhouse Gas Control 5 (2011) 659-667.

[10] J. Adánez, P. Gayán, J. Celaya, L.F. de Diego, F. García-Labiano, A. Abad. Chemical Looping Combustion in a 10 kW_{th} Prototype Using a CuO/Al_2O_3 Oxygen Carrier: Effect of Operating Conditions on Methane Combustion. Ind. Eng. Chem. Res. 45 (2006) 6075-6080.

[11] L.F. de Diego, F. García-Labiano, P. Gayán, J. Celaya, J.M. Palacios, J. Adánez. Operation of a 10 kW_{th} chemical-looping combustor during 200 h with a $CuO-Al_2O_3$ oxygen carrier. Fuel 86 (2007) 1036-1045.

[12] A. Lambert, A. Tilland, W. Pelletant, S. Bertholin, F. Moreau, I. Clemençon, M. Yazdanpanah. Performance and degradation mechanisms of CLC particles produced by industrial methods. Proc. 4^{th} Int. Conf. Chemical Looping (2016) Nanjing, China.

[13] S. Penthor, K. Mayer, S. Kern, H. Kitzler, D. Wöss, T. Pröll, H. Hofbauer. Chemical-looping combustion of raw syngas from biomass steam gasification - Coupled operation of two dual fluidized bed pilot plants. Fuel 127 (2014) 178-185.

[14] S. Penthor, F. Zerobin, K. Mayer, T. Pröll, H. Hofbauer. Investigation of the performance of a copper based oxygen carrier for chemical looping combustion in a 120 kW pilot plant for gaseous fuels. Applied Energy 145 (2015) 52-59.

[15] K. Mayer, S. Penthor, T. Pröll, H. Hofbauer. The different demands of oxygen carriers on the reactor system of a CLC plant - Results of oxygen carrier testing in a 120 kW_{th} pilot plant. Applied Energy 157 (2015) 323-329.

[16] Ø. Langørgen, I. Saanum, N.E.L Haugen. Chemical looping combustion of methane using a copper-based oxygen carrier in a 150 kW reactor system. Energy Procedia 114 (2017) 352-360.

[17] R.F. Pachler, M. Kollerits, K. Mayer, S. Penthor, H. Hofbauer. Fate of sulfur in chemical looping combustion of gaseous fuels using a copper based oxygen carrier. Proc. 4th Int. Conf. Chemical Looping (2016) Nanjing, China.

[18] S.P. Sit, A. Reed, U. Hohenwarter, V. Horn, K. Marx, T. Proell. Cenovus 10 MW CLC Field Pilot. Energy Procedia 37 (2013) 671-676.

[19] A. Abad, J. Adánez, F. García-Labiano, L.F. de Diego, P. Gayán. Modeling of the chemical-looping combustion of methane using a Cu-based oxygen-carrier. Combustion Flame 157 (2010) 602-615.

[20] A. Abad, P. Gayán, F. García-Labiano, L.F. de Diego, J. Adánez. Relevance of Oxygen Carrier Characteristics on CLC Design for Gaseous Fuels. 3rd International Conference on Chemical Looping (2014) Göteborg, Sweden.

[21] A. Abad, J. Adánez, F. García-Labiano, L.F. de Diego, P. Gayán, P. Kolbitsch, T. Pröll. CLC Modeling: the fuel-reactor at fast fluidization – Conversion of CH_4 using a NiO-based oxygen-carrier in a 120 kW_{th} unit. Proc. 1st Int. Conf. Chemical Looping (2010) Lyon, France.

[22] A. Abad, P. Gayán, L.F. de Diego, F. García-Labiano, J. Adánez. Modelling a CLC process improved by CLOU and validation in a 120 kW unit. Proc. 11th Int. Conf. Fluidized Bed Technology, CFB-11 (2014) Beijing, China.

[23] A. Abad, J. Adánez, L.F. de Diego, P. Gayán, F. García-Labiano, A. Lyngfelt. Fuel reactor model validation: Assessment of the key parameters affecting the chemical-looping combustion of coal. Int. J. Greenhouse Gas Control 19 (2013) 541-551.

[24] D. Kunii, O. Levenspiel. Circulating fluidized-bed reactors. Chem. Eng. Sci. 52 (1997) 2471-2482.

[25] D. Kunii, O. Levenspiel. Fluidized Reactor Models. 1. For Bubbling Beds of Fine, Intermediate, and Large Particles. 2. For the Lean Phase: Freeboard and Fast Fluidization. Ind. Eng. Chem. Res. 29 (1990) 1226-1234.

[26] F. Johnsson, S. Andersson, B. Leckner. Expansion of a freely bubbling fluidized bed. Powder Technol. 68 (1991) 117-123.

[27] D. Pallarès, F. Johnsson. Macroscopic modelling of fluid dynamics in large-scale circulating fluidized beds. Prog. Energy Combust. Sci. 32 (2006) 539-569.

[28] A. Abad, P. Gayán, L.F. de Diego, F. García-Labiano, J. Adánez. Fuel reactor modelling in chemical-looping combustion of coal: 1. model formulation. Chem. Eng. Sci. 87 (2013) 277-293.

[29] S. Furusaki, T. Kikuchi, T. Miyauchi. Axial Distribution of Reactivity Inside a Fluid-Bed Contactor. AIChE J. 22 (1976) 354-361.

[30] F. García-Labiano, L.F. de Diego, J. Adánez, A. Abad, P. Gayán. Temperature variations in the oxygen carrier particles during their reduction and oxidation in a chemical-looping combustion system. Chem. Eng. Sci. 60 (2005) 851-862.

[31] A. Abad, J. Adánez, F. García-Labiano, L.F. de Diego, P. Gayán, J. Celaya. Mapping of the range of operational conditions for Cu-, Fe-, and Ni-based oxygen carriers in chemical-looping combustion. Chem. Eng. Sci. 62 (2007) 533-549.

[32] V. Kempkes, A. Kather. Thermodynamic analysis of a coal fired chemical looping combustion power plant. 5th Int. Conf. Clean Coal Technologies (2011) Saragossa, Spain.

[33] A. Lyngfelt, B. Leckner. A 1000 MW_{th} boiler for chemical-looping combustion of solid fuels - Discussion of design and costs. Applied Energy 157 (2015) 475-487.

[34] E.U. Hartge, K. Redemann, J. Werther. The bed inventory of the Duisburg CFB combustor - measurement and simulation. 55th IEA-FBC Meeting: Corrosion, Ash and Modelling (2007) Paris, France.

[35] A. Cabello, P. Gayán, F. García-Labiano, L.F. de Diego, A. Abad, J. Adánez. On the attrition evaluation of oxygen carriers in Chemical Looping Combustion. Fuel Process. Technol. 148 (2016) 188-197.

[36] M. Rydén, P. Moldenhauer, S. Lindqvist, T. Mattisson, A. Lyngfelt. Measuring attrition resistance of oxygen carrier particles for chemical looping combustion with a customized jet cup. Powder Technol. 256 (2014) 75-86.